First Processing of the Complete Sentinel-1 SAR Archive: 10 Years of Global Sea State

Andrey Pleskachevsky, Björn Tings, Christoph Schnupfhagn, Stefan Wiehle, and Sven Jacobsen

***Abstract*—In this study, the sea state was estimated and analyzed by processing the ten-year worldwide Sentinel-1 synthetic aperture radar (SAR) archive 2014−2024. The approx. 15 Petabytes of data contain approx. 4.2 million SAR scenes, where approx. 3 million are Interferometric Wide Swath (IW, acquisitions mainly in shelves and seas), approx. 1 million Extra Wide Swath (EW, mainly poles but also Atlantic, Madagascar) and approx. 0.2 million Wave Mode (WV, open oceans) products. Eight integrated sea state parameters are derived: total significant wave height (SWH), first and second moment wave periods, mean wave period, dominant and secondary swell wave heights, and windsea wave height and periods. The sea state parameters are provided on a 5 km grid for IW, a 17.5 km grid for EW, and by average values for WV's along-flight imagettes. The validations were carried out with reanalysis model results and buoys. The empirical algorithm SAR-SeaStaR uses machine learning and was improved by extending the training data with extreme storms and buoy collocations. Furthermore, worldwide areas with increased ground truth uncertainties, identified by big differences between data sources, were identified and excluded from training. This approach results in an improved worldwide SWH root mean square error of 0.38 m for S1 IW and 0.45 m for S1 EW by model comparison. The results of all three S1 modes cover the entire globe, including open ocean, shelves, and internal seas, and are being made available for the public through the European Space Agency in the framework of the Climate Change Initiative - Sea State ECV project. They can be used for analysis and statistics of the worldwide sea state. A first exemplary analysis of the global S1 data shows a slight increase in the percentage of low sea state, with a corresponding decrease in high sea by approx. 2% of the total in shelf areas (dominant data in the North Atlantic) and seas (Mediterranean, North, Baltic, Black Seas, etc.), but an increase in very high storms in the open ocean by approx. 0.3% in the last ten years. The storms at the Cape of Good Hope in South Africa weakened, while storms off Cape Horn in South America intensified.**

***Index Terms*—Integrated sea state parameters, SAR-SeaStaR, Sentinel-1 archive, synthetic aperture radar (SAR).**

I. INTRODUCTION

A. SAR Processing for Meteo-Marine Parameters Estimation

MORE than 70% of the Earth's surface is covered by oceans, where surface waves transfer the energy obtained from the atmosphere. Changes in the energy balance in the atmosphere also cause a change in sea state development, propagation, and distribution in space and time. Today, to evaluate the change in the global sea state, there are a series of opportunities by using modern instruments and techniques: numerical modeling reanalysis, in-situ measurements, and remote sensing data. One of the remote sensing instruments is satellite-borne synthetic aperture radar (SAR). The advantage of this device is that SAR, as an active sensor, is independent of daylight, has global coverage, and can capture a footprint of 20–450 km, depending on mode, providing continuous sea state fields that represent the local wave distribution. The disadvantage, compared to other space-based instruments, is that the SAR data are large—on the order of several GB per scene—and require a certain amount of time and capacity to be transmitted to a ground station (GS) where they are then processed. The ability to process this large amount of data quickly is one of the main requirements for the processing algorithms, especially when it comes to Near Real Time (NRT) processing. Also, the processing of large archives was not possible for all SAR data in the past, and only with the latest developments of the methods and supercomputer infrastructures has such work become possible in recent years.

Fig. 1 shows an example of the sea state for one day of processed acquisitions from European Space Agency (ESA) Sentinel-1 (S1) SAR satellites S1-A and S1-B [1], covering the globe. The three main acquisition modes considered in this study are as follows.

1) Wave mode (WV) acquired over open oceans, along-orbit imagettes approx. 20 × 20 km every 100 km.
2) Interferometric Wide Swath mode (IW) in shelf regions and seas, strips up to 2000 km with a swath width of approx. 250 km.
3) Extra Wide Swath mode (EW) in polar regions with a swath width of approx. 450 km.

During processing at GSs, the IW and EW raw data are divided into images with individual product IDs along the flight length of approx. 200 km for IW and approx. 400 km for EW and converted into Level-1 (L1) products for easier distribution. This dividing can differ depending on the processing of the raw SAR data at different GSs.

In the exemplary day 2021-01-01 (Fig. 1), approx. 750 products containing ocean/seas were acquired, resulting in approx. 5 70 000 water data points processed with SAR-SeaStaR algorithm [2]: 513 IW products (5 km processing raster), 212 EW products (17.5 km processing raster), and 59 WV tracks with a total amount of approx. 1.5 TB of original data [S1 Ground Range Detected (GRD) ESA L1 products].

Received 14 November 2025; revised 4 February 2026; accepted 2 March 2026. Date of publication 10 March 2026; date of current version 30 March 2026. This work was supported in part by the European Space Agency (ESA) within the Climate Change Initiative CCI+ project CCI-SeaState [23]. *(Corresponding author: Andrey Pleskachevsky.)*

The authors are with the German Aerospace Center DLR, Earth Observation Center, Maritime Safety and Security Lab Bremen, 28359 Bremen, Germany (e-mail: andrey.pleskachevsky@dlr.de).

Digital Object Identifier 10.1109/JSTARS.2026.3672664

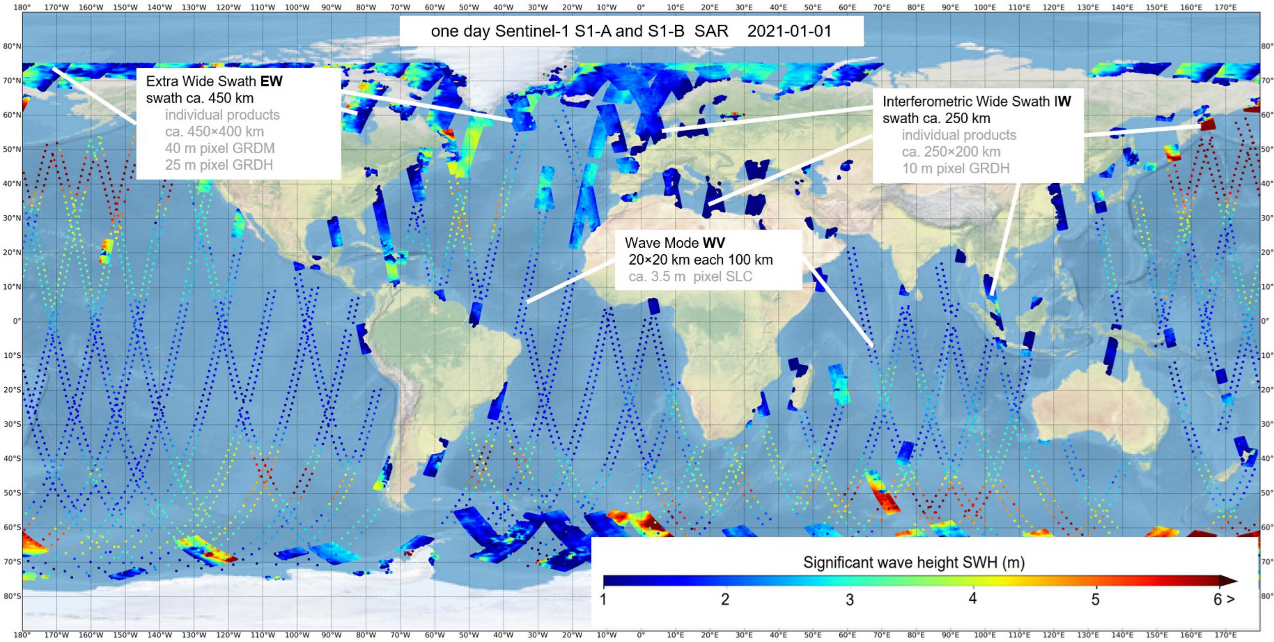

Fig. 1. Example of one-day sea state estimated from Sentinel-1 satellites S1-A and S1-B in the scope of this study on 2021-01-01. The three main acquisition modes, WV, along-flight imagettes, IW, and EW scenes, are acquired in different areas with switched acquisition modes. The acquired IW and EW raw data are divided into individual products with an along-flight length of approx. 200 km for IW and approx. 400 km for EW. In total, 748 products with approx. 5 70 000 processed water points are shown: 59 WV tracks (averaged values for an imagette 20 × 20 km), 513 S1 IW products (5 km processing raster), 212 EW products (approx. 17.5 km processing raster).

In the context of modern developments, the following four main points should be considered during algorithm design.

1) *Scientific approaches:* Algorithms and models used for the description of the physics or empirical relations for the derivation of the parameters.
2) *Methodology:* cthe way the models are mathematically solved and implemented. These include, e.g., the older linear regression (LR)-based solutions and the newest machine learning (ML) approaches. The data selection for training and validation also plays a key role.
3) *Technical implementation of the methods:* Enabling their practical applications (e.g., NRT services or academic studies), using high-performance software libraries and supercomputers.
4) *Application requirements:* For some algorithms, accuracy is the focus of development, for others, applicability and processing speed are the priority.

In terms of scientific approaches, the algorithms are developed for different purposes and processing conditions. Two basic approaches have been identified for sea state SAR applications: One approach is specifically designed to reconstruct wave spectra (swell spectrum in the first place) using transfer functions (e.g., [3]). The other approach is using empirical methods specifically designed for quick estimation of integrated parameters like significant wave height (SWH) directly from SAR image intensities without spectral transformations (e.g., [4] and [5]). Both methods have advantages and disadvantages: The wave-spectrum-based methods can deliver directional information and can be used for numerical model assimilation (e.g., [6] and [7]). However, spectral transformations can only be applied for acquisitions where wave patterns are imaged in SAR scenes. This method works properly in open oceans where the long swell waves with wavelengths in the order of hundreds of meters exceed the so-called *cut-off* for SAR wave imaging (approx. 120−150 m for S1) [8], [9]). However, in coastal areas and seas, where the S1 IW scenes are acquired, the sea state is dominantly shorter with approx. 80% of all acquisitions with wavelengths under 120 m (statistics will be shown in Section II, Fig. 3). Although the empirical methods do not provide a wave spectrum, they are applicable to almost all circumstances (coastal scenes with ships, wakes, low wind, very short waves, etc., nonvalid data are approx. 1.5%), with high processing speed and high SWH accuracy (examples in next paragraph on methodology) [10]. They are designed for NRT processing and services where the current sea state information is directly provided to users, such as ship officers or weather services. For example, the sea state from S1 IW 250 × 200 km images with a 3 km raster step (approx. 5000 subscenes) is processed at the GS Neustrelitz, operated by German Aerospace Center (DLR). The surface wind and sea state parameters from S1 IW images in the North and Baltic Seas are daily, fully automated, and take around 3 min [11]. Such an approach also allows a fast processing of large amounts of archived data (more details see in Section II).

In terms of methodology, the application of ML techniques and the availability of large archive datasets in the last few years made the accuracy of the estimation methods comparable to the statistical uncertainties in the ground truth data (buoys, hindcasts). Just a few years ago, ML approaches provided solutions comparable to classical approaches based on LR. For example, the accuracy of SWH estimated from S1 WV imagery by using neural networks (NNs) in 2017 delivered root mean square errors (RMSEs) of about 0.50 m, which is not different from the widely known and approachable LR CWAVE method [12]. However, in 2020, the accuracy of ML methods was improved to 0.35 m by applying a deep learning (DL) method [13], and in later studies, achieved an accuracy of approx. 0.25−0.28 m for different ML approaches [13], [14], [15]. Today, ML methods allow increasingly accurate results also for other satellites, e.g., for the Chinese Gaofen-3 mission (three satellites launched in 2016, 2021, 2022 with an altitude of approx. 755 km), C-Band SAR WV imagettes can be processed with good consistency in terms of an RMSE of 0.32 m by applying a deep residual convolutional NN [16]. For the TerraSAR-X/TanDEM-X mission (launched in 2009 and 2011 with an altitude of approx. 514 km) with X-band SAR StripMap data acquired mostly in extremely short waters, an accuracy of approx. 0.35 m was reached [2].

The accuracy of the methods by their whole worldwide application (different from limited application in a selected area, e.g., only in Atlantic or only for selected storms) varies depending on the satellite type/mode (in terms of X or C radar bands, satellite altitude, and SAR image resolution) and acquisition area. The latter is caused by the fact that in different regions of the world, the ground truth data, based predominantly on hindcast modeling (worldwide buoys are located mostly in shelfs and coastal areas and do not cover oceans and complex areas such as South Africa with the Cape of Good Hope), has different uncertainties, which depend on the physics, atmospheric input and spatial resolution of different models [17], [18]. For example, using different methods (support vector machine (SVM) in [14] and DL in [15]), the state-of-the-art worldwide accuracy for S1 WV of ESA Sentinel-1 satellites for SWH in open ocean is RMSE∼0.27 m. At the same time, the uncertainty between the MFWAM (Météo-France Wave Model [19]) and WW3 (WaveWatch-3 model of the National Oceanic and Atmospheric Administration (NOAA) [20]) spectral numerical model hindcast against the National Data Buoy Center (NDBC) buoys is also approx. 0.28 m at the NOAA wave rider locations [21]. Furthermore, in shelf and coastal areas, where wavelengths are very short, the waves cannot be imaged from space individually and only appear as noise in SAR; the sea state estimation methods have a more difficult task. In addition, in coastal areas, numerous artifacts in SAR signatures, such as ships, ship wakes, oil, offshore construction, buoys, seamarks, etc., are present, which have to be filtered. The filtering, denoising, and control procedures are an integral part of the algorithms, influencing the results by approx. 30%, but these cannot eliminate all artifacts when processing millions of real scenes [2], [10].

From a technological perspective, computer performance has improved significantly in recent years, enabling the processing of larger SAR data archives on supercomputers by executing hundreds of parallel processes. This jump in developments of the processing infrastructure means that tens of thousands of SAR images can now be processed and analyzed in a short time. For example, in 2020, the authors needed approx. three weeks to process one year of acquisitions from the S1 WV original Single-Look Complex (SLC) product archive. In the scope of this work, using the Leibniz Supercomputing Centre (LRZ) [22], this data volume was processed in three days.

From an application perspective, several points set the boundary conditions for method development. For applicability, not only the accuracy in terms of RMSE and bias (BIAS) must be considered, but also the percentage of rejected values (“bad_value” flag), outliers, and processing speed are optimization parameters. For example, filtering out the uncertain scenes (e.g., with artifacts or noisy images) improves the total accuracy, but increases the percentage of unprocessed data. Therefore, not only the accuracy of the model function in terms of RMSE, but also the methods for filtering and outlier detection must be optimized.

B. *Objective of the Study*

In this study, the following three main points were addressed.

1) Improvement of the S1 IW and EW sea state retrieval method. This concerns the improvement of the method accuracy under the condition that all existing scenes can be processed with a low percentage of invalid data points, working with different types of SAR data (concerns EW mode), and adopting the algorithm as a sea state processor (SSP) for working on supercomputer infrastructures.
2) Processing the S1 archive in terms of integrated sea state parameters and arranging a worldwide database to be included in the ESA CCI (Climate Change Initiative [23]) sea state climate change analysis.
3) A first analysis of the sea state statistics in terms of distribution and redistribution of the low, moderate, and high sea states worldwide on processed S1 data.

The rest of this article is organized as follows. In Section II**,** the data, methodology, and processing of the S1 archives are described. Section III deals with the improvement of the method for IW and EW S1 modes. The questions of the uncertainties in ground truth data and the impact of the buoy collocation distance on the results are discussed, and an exemplary statistical analysis of the wave height redistribution over ten years based on S1 data is presented. Section IV summarizes the study.

II. DATA AND METHODS

A. *Sentinel-1 Data and Processed Parameters*

In the scope of this work, the whole worldwide ten-year Sentinel-1 SAR archive from C-band Copernicus S1-A and S1-B satellites [1] was processed in terms of sea state. The data starts in November 2014 with S1-A. The amount of data doubled from the start of data delivery from S1-B in 2016 until its end-of-service in late 2022. The sea state from the following three main modes was processed (both S1-A and S1-B in service).

1) *WV:* approx. 100 imagettes 20 × 20 km every 100 km across oceans with approx. 7 GB/pass, approx. 60 passes/day.
2) *IW:* one image product coverage approx. 250 × 200 km with approx. 2 GB, approx. 600 images/day.

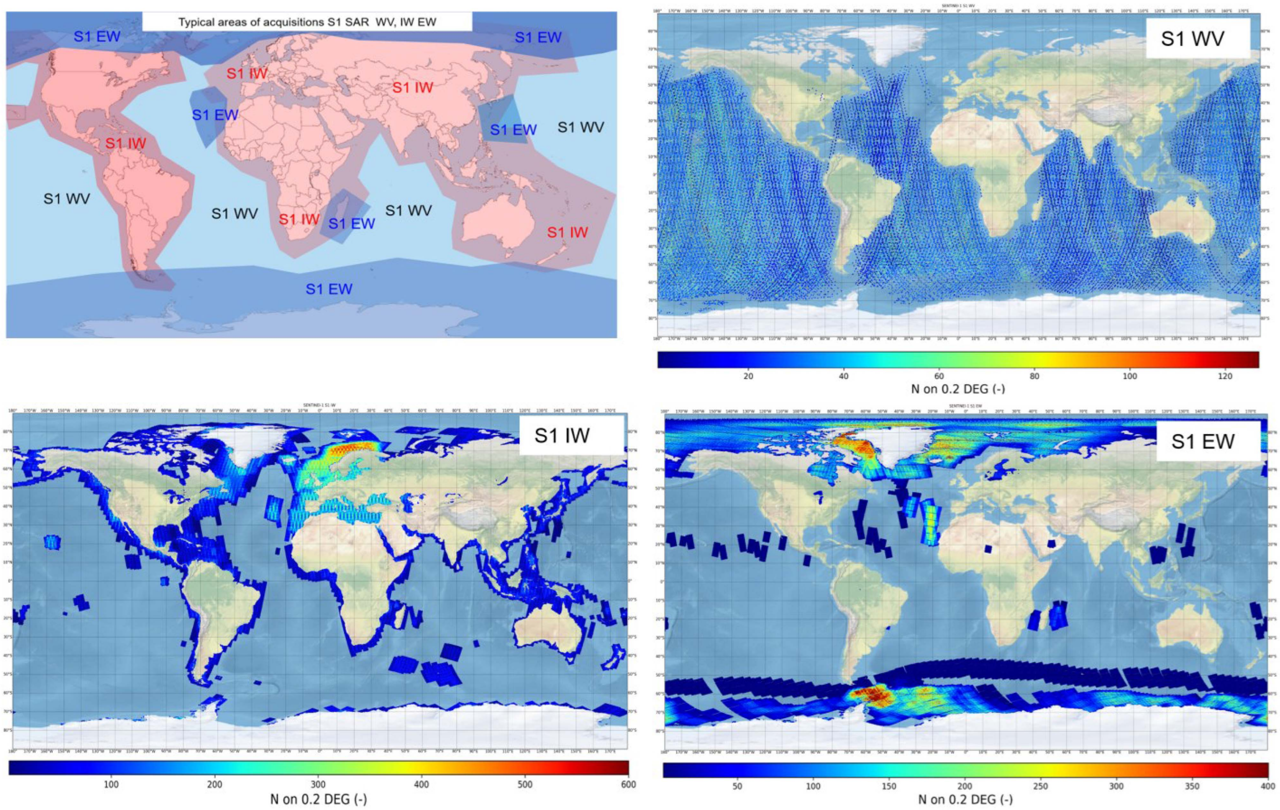

Fig. 2. Scheme of Sentinel-1 SAR ocean acquisition areas: IW (red), EW (blue), and WV (top left). Example one-year data in 2020 (both S1-A and S1-B in service) WV, IW EW, color means density of processed data on 0.2° mesh: 20 km imagettes every 100 km for WV along orbits, 5 and 17.5 km raster for IW and EW, respectively.

3) *EW:* one image product coverage approx. 450 × 400 km with approx. 1 GB, approx. 260 images/day.

For processing, for WV, the SLC, and for IW and EW, the GRD ESA Level-1 products were used [1]. The detailed information on product characteristics and processing details can be seen in Appendix Table VII.

Initially, from the scene ID alone, it is not possible to determine the proportion of water points and which scene is entirely on land. Therefore, all available archive scenes were processed; later, only scenes with at least 2 km of water area were designated as ocean scenes and included in the sea state products (DLR_OCN). This complicates the processing, as only approx. 40% of all archive data covers water, but all of it must first be processed and evaluated: the WVs are only recorded over oceans, while only approx. 40% of all IW and approx. 80% of all EW scenes include the seas and ice-free open water.

Fig. 2 demonstrates an example of the acquisition distribution around the world in 2020 when both S1-A and S1-B were in service (the processed data are projected on a 0.2° mesh corresponding to the sea state reanalysis model used in the study, description in the next paragraph "Ground truth data"). In Fig. 3, the statistical distribution of SWH and approximate wavelengths evaluated from wave periods in Sentinel-1 data for different modes is shown. The distributions are calculated with 0.25 bins in meters for SWH and seconds for period transferred into wavelength using the deep-water dispersion relation. The IW acquisitions in shelves and seas have around 70% of all data with SWH$<$2 m and wavelength$<$120 m (corresponds to *cut-off* and means only approx. 30% of all IW data can be applied to spectral transformation methods, e.g., [3]). Vice versa, the open-ocean WV acquisitions have around 70% of all data with SWH$>$2 m and wavelength$>$120 m. The EW in polar regions builds a middle case.

The results are the eight integrated sea state parameters: total SWH, wave heights of dominant and secondary swells and windsea, mean, first and second moment wave period TM2, and windsea period. SAR scenes are processed in raster format, and the output is fields for each parameter showing their spatial distribution.

Every day, approx. 400 IWs, approx. 200 EWs and approx. 60 WV were acquired over the oceans. In total, for 10 years, approx. 13 million IW scenes with approx. 1.3 billion data points (5 km processing raster), approx. 0.5 million EW with approx. 0.3 billion data points (17.5 km processing raster) and ca. 1 70 000 WV with ca. 15 million data points were processed. All processed data were collocated and validated with wave model hindcasts and buoys for $-50^\circ < \mathrm{LAT} < 60^\circ$ (avoiding ice coverage). All results are stored as netCDF-formatted DLR ocean products (DLR_OCN), including uncertainties and quality flags, and provided to ESA for public use.

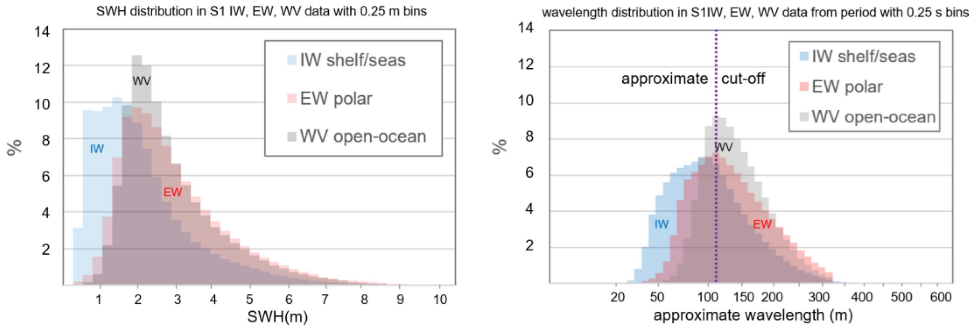

Fig. 3. Distribution of SWH (left) and approximate wavelength (right) evaluated from wave period in Sentinel-1 data with 0.25 m bins. The IW acquisitions in shelf and seas have around 70% of all data with SWH$<$2 m and wavelength$<$120 m, the open-ocean WV acquisitions have vice versa, around 70% of all data with SWH$>$2 m and wavelength$>$120 m. The EW in polar regions builds a middle case.

B. Ground Truth Data

For trainings and validations, numerical worldwide sea state hindcasts and local in-situ measurements from wave rider buoys were used. The integrated parameters from the following two hindcast wave models were considered.

1) MFWAM reanalysis. MFWAM results are available with a spatial resolution of 1/5°[19], [24].
2) WW3 model of NOAA with a spatial resolution of 1/2° [20].

The results of both models are provided in 3-h steps and are temporally interpolated (tests without temporal interpolation used for training resulted in approx. 3 cm lower RMSE by validations with buoys [10]). In the previous study [2], it was shown that MFWAM as ground truth results in better validation results with buoys than using WW3 and also mixed MFWAM/WW3 data (which can be explained by differences in the models' spatial resolutions, especially in coastal areas). For this reason, MFWAM was taken as a training source, and WW3 was applied for comparisons with MFWAM to determine the areas with increased uncertainty.

As an independent source, the in-situ data provided from different operators with focus on the NDBC, Environment and Climate Change Canada (ECCC), and European Marine Observation and Data Network (EMODNET) [21], [25], [26] were used. In total, 182 buoys providing sea state measurements and collocated to S1 acquisitions were found worldwide for $-50° < \mathrm{LAT} < 60°$ ice-free area within a distance of $>$10 km from the coasts. However, for the polar EW mode, the buoys around Iceland at about 64°N were also considered as the only collocation possibility. Only buoy records with a maximum time gap between measurements of 6 h (some buoys have failed for months) have been used, where the SAR acquisition is between two measurements.

The uncertainty in the ground truth was evaluated in [2] with approx. 0.26 m for wave height SWH (RMSE approx. 0.26 m for MFWAM/NDBC, approx. 0.25 m for MFWAM/WW3 at NDBC buoy locations, and approx. 0.35 m worldwide).

C. Methodology

The Sentinel-1 SAR archive was processed using the empirical SAR-SeaStaR algorithm implemented into the SSP as a part of the SAINT (SAR AIS Integrated Toolbox) software package [2], [9]. In the scope of this study, the algorithm was improved for S1 IW and EW modes (details in Section III-A and C). The algorithm was developed for NRT use. It applies a combination of a classical approach using LR with ML by applying the SVM technique [27]. For the study, the high-performance ThunderSVM (TSVM) library was used, which runs an order of magnitude faster than the standard LibSVM [28]. The method is based on an analysis of subscenes by estimating several SAR features from the Normalized Radar Cross Section (NRCS). After denoising, prefiltering, and the control-of-features operations, these features are directly used in a model function to estimate the sea state parameters without intermediate transfer into wave spectra. The primary SAR features are estimated from radiometrically calibrated, filtered, denoised, land-masked, and normalized subscenes with a size of 1024 $\times$ 1024 pixels and are of the following five types.

1) NRCS and NRCS statistics (variance, skewness, kurtosis, etc.).
2) Geophysical parameters (surface wind speed estimated from analyzed subscene using CMOD-5 algorithms for C-band [29]).
3) Gray level co-occurrence matrix parameters (homogeneity, dissimilarity, etc.).
4) Spectral parameters based on integration of image spectrum obtained using fast Fourier transformation in wavenumber k domain for different wavelength domains (0–30, 30–100, 100–400 m, etc.) and spectral width parameters.
5) Spectral parameters using products of normalized image spectrum with orthonormal functions (CWAVE approach) and cut-off wavelength estimated using the autocorrelation function.

In total, 54 primary features are applied. A more detailed description of the features can be found in [2], [5], and [10]. The method is created using a modular architecture, including a series of filtering and control procedures, as well as a series of LR and ML model functions for different satellites/modes. With an extended database, the model functions can be retrained and replaced in the SSP. Special attention is paid to stability and applicability of the algorithm under all conditions (e.g., for low winds under 1.5 m s^{-1}). For example, the number of nonvalid ocean scenes/subscenes for S1 WV is approx. 1.5% with an accuracy of approx. 0.26 m in terms of SWH. In comparison,

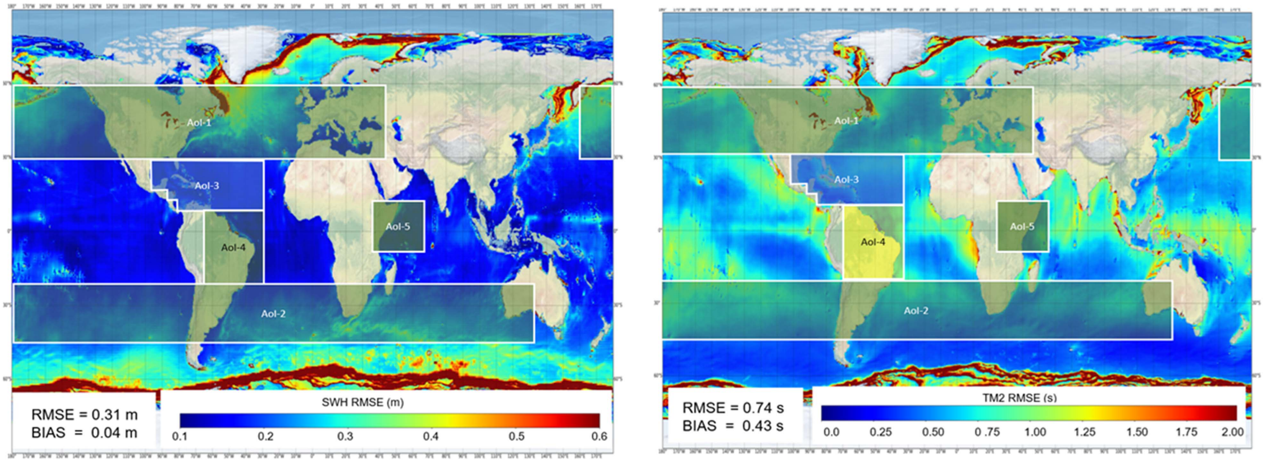

Fig. 4. Example comparison between the two wave model results (SWH on left, TM2 period on right) and area-of-interests used for retraining the model function. The strongest variations between models are due to the different ice masks in the models. Based on the amount of IW scenes in different regions, the areas of the west coasts of Africa and Middle America, as well as around India, the Philippines, and eastern Australia, provided the largest contribution to the method inaccuracies. Five AoIs were implemented for retraining of the model functions.

the same S1 WV data processed using a comparable algorithm [15] results in the same RMSE of 0.26 m but with approx. 13.5% of all data was rejected as invalid.

D. Processing the Sentinel-1 SAR Archives

The processing was executed on the Terrabyte cluster at LRZ [22]. The huge amount of approx. 15 Petabytes (PBs) of data (approx. 4 million S1 IW and EW products) requires the usage of such a supercomputing system enabling large-scale parallel processing. Technically, the scenes were separated to process one day of data in one job; one year was processed in 365 parallel jobs. The most extensive processing of S1 IW (approx. 1500 subscenes/product, approx. 900 products/day) takes about one week for a year, including queuing time. The processing was carried out in the following way.

1) *S1 IW:* The years 2014–2023 were processed using model functions based on [2], the data of 2024 were processed using an improved model function (see later).
2) *S1 EW:* The processing of the entire EW 2014–2024 archive was carried out (in the previous studies [2], exemplary data were considered) using the model function retrained in the scope of this study.
3) *S1 WV:* The S1 WV data for 2014–2020 were already processed in the scope of ESA CCI-1 [2] and are publicly available [14]. In this work, the rest of the data 2021–2024 was processed.

Table VIII in the Appendix gives an overview of the complete processed ocean scenes for S1 IW, EW, and WV included in the resulting DLR_OCN products after excluding land scenes.

III. RESULTS

A. Processing and Improvement of S1 IW

As already mentioned in Section I, S1 IW mode covers the ocean surface in strips of up to 2000 km with swaths of approx. 250 km and are divided into L1 products with approx. 200 km along-flight length. The GRD IW products have a pixel spacing of 10 m and are processed with a raster of 5 km corresponding to approx. 1500 datapoints per product (see Table VII).

In the first phase, the S1 IW archive 2014–2023 was processed, and using the SAR-SeaStaR algorithm with model functions published in [2], the results were delivered to ESA through CCI.

The processed archive was applied to extend the training datasets (the processed SAR features were stored and collocated with the ground truth data). Due to the large amount of processed data with approximately 1 billion data points, this is the first study in which the buoy collocations were used for training purposes in a large volume, with a magnitude of 0.5 million points.

In the next step, the uncertainties between different numerical hindcast models were analyzed. It has been recognized by validation for individual regions of the Earth that there are areas with higher and lower RMSE values between the ground truth sources. In this study, the RMSE for SWH and the second moment wave period (TM2) between three models was analyzed. The areas with stronger uncertainty between the models were defined and excluded from training. Analyzed were the WW3 model and the MFWAM reanalysis.

Fig. 4 presents an example of RMSE calculated for one-year data (3-h outputs) between MFWAM and WW3. The strongest variations between models can be seen in polar regions due to the different ice masks in the models. Due to strong storms in the North Atlantic and the South Indian Ocean with SWH often exceeding 10 m, the RMSE is higher, but not noticeable in terms of percentage (scatter index SI). From a remote sensing perspective, the use of model data in these areas is similar to the use of data in regions with full or partial ice coverage, where model uncertainty is higher. The exclusion of ice-coverage areas is standard in similar scientific studies, e.g., [10], [12], and [13].

TABLE I
ANALYSIS OF THE SWH FOR THE S1 IW ARCHIVE 2024 PROCESSED WITH 5 KM RASTER USING MODEL FUNCTIONS DEVELOPED IN THE PREVIOUS STUDY [2] (OLD) AND IN THIS STUDY (NEW) COMPARED TO MFWAM MODEL RESULTS

Sea state domain (m)	RMSE (m)		BIAS (m)		N collocations (active points)	Data distribution %
	Old With [2]	**New This study**	Old With [2]	**New This study**		
0.0<SWH<1.5	0.32	**0.29**	–0.17	**–0.10**	39 911 563	50.62
1.5<SWH<3.0	0.38	**0.37**	0.03	**–0.02**	29 876 514	37.85
3.0<SWH<6.0	0.63	**0.58**	0.22	**0.04**	8 419 847	10.64
SWH>6.0	1.10	**0.77**	0.57	**0.19**	700 774	0.89
TOTAL	0.42	**0.38**	–0.03	**–0.03**	78 908 698	100.00

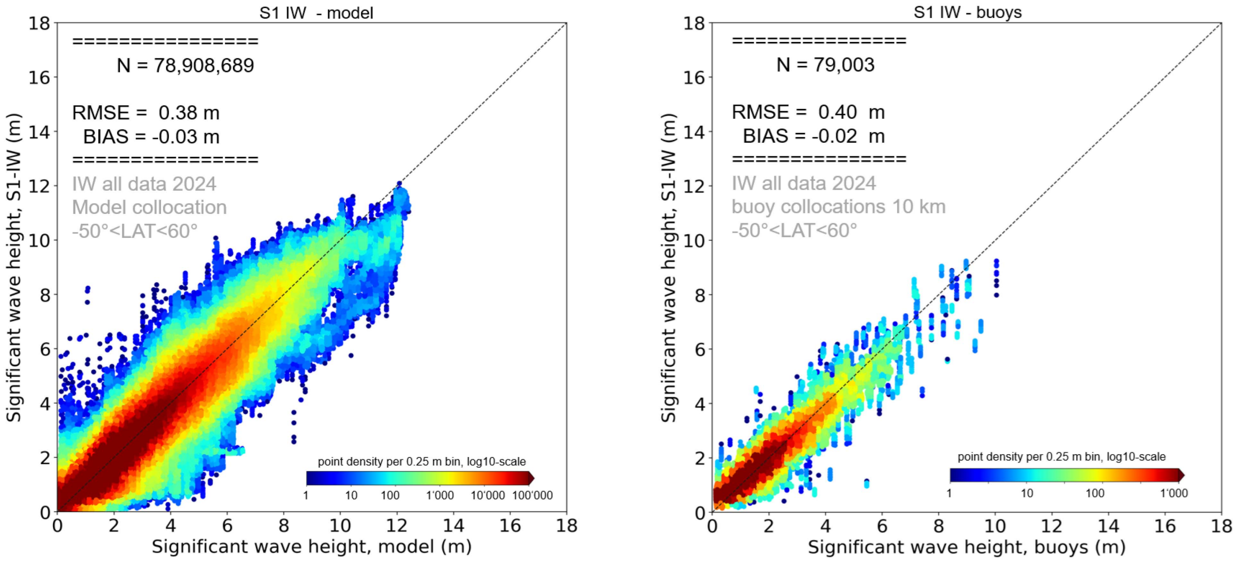

Fig. 5. SWH comparison with model and buoys for worldwide S1 IW data in 2024. All archived S1 IW scenes −50°<LAT<60° with approx. 1 13 000 IDs, approx. 80 million model collocations and approx. 80 000 buoy collocations.

Considering the amount of worldwide IW acquisitions, the areas of the west coasts of Africa and middle America, as well as around India and the Philippines and eastern Australia, provided the largest contribution to the uncertainties in the training. For the retraining of the model functions, five AoIs were implemented (see Fig. 4).

The training dataset was created with approx. 2 million datapoints. Here, approx. 1 million points were collected using all scenes in the AoIs 2015−2018. From 2019, the data with SWH>6 m (0.5 million points) and buoy collocations under 10 km (0.5 million points) are collected. The retrained model function for SWH was validated with the S1 IW complete archive 2024 (all existing scenes without exceptions in the area −50°<LAT<60°). Using the original function [2] results in an RMSE of 0.42 m, the new retrained function in 0.38 m by using the same validation model data (approx. 80 million collocations). Table I presents the results of the validations.

The most significant improvements were achieved for high sea state (RMSE 0.77 m against 1.10 m in the previous study [2]). The total deviation remains the same with BIAS = −0.03 m. However, BIAS was significantly improved for high sea state (0.19 m against 0.57 m for SWH>6 m). Fig. 5 shows the SWH comparison with the model and buoys. As EMODNET [23] provides data for more buoys since 2024, the number of collocated buoys was extended to 242. The buoy comparisons with a 10 km collocation distance result in approx. 7 cm improvements in comparison to the previous study [2].

Table II shows the cross-comparison for three combinations of data sources: SWH of DLR_OCN, buoys, and the MFWAM model (only buoy locations). Fig. 6 visualizes the table. The uncertainty for all sources increases with the wave height. The averaged extrapolated uncertainty can be assessed as *uncertainty* = 0.20+0.10·SWH (i.e., 20 cm ground noise with an additional 10% of the SWH value).

B. Effect of Buoys Collocation Distance and Radius on Results Uncertainty

The global S1 IW archive, which has been compiled over several years, offers the opportunity for the first time to conduct a study on the sensitivity of the results to the collocation radius using several million data points. For four years 2019−2022, the buoy collocations were analyzed with different collocation distances. The collocation radius was extended from 1 km

TABLE II
SWH CROSS COMPARISON BETWEEN DLR_OCN, BUOYS, AND MODEL (ONLY BUOY LOCATIONS)

Wave height domain (m)	Model–S1 IW (m)	Buoys – S1 IW (m)	Buoys – model (m)	N	%
0.0 < SWH< 1.5	0.23	0.30	0.20	33 019	51.84
1.5 < SWH< 3.0	0.38	0.40	0.29	22 614	35.51
3.0 < SWH< 6.0	0.55	0.61	0.48	7515	11.80
6.0 < SWH	0.98	1.02	0.76	544	0.85
TOTAL	**0.38**	**0.40**	**0.29**	**63 692**	**100.00**

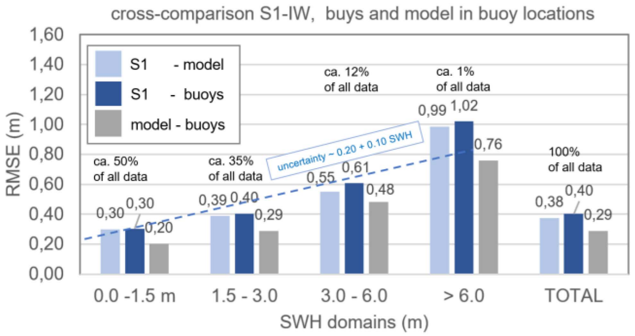

Fig. 6. Cross comparison of SWH for DLR_OCN, buoys, and model (only buoy locations). The uncertainty for all sources grows with a higher value of the wave height. The averaged extrapolated uncertainty can be assessed as *uncertainty* = 0.20+0.10·SWH.

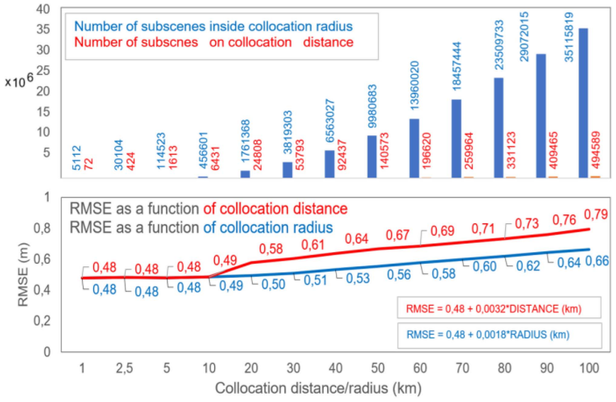

Fig. 7. Top: Collocation of the S1 IW archive to 181 NDBC and EMODNET buoys 2019–2022 processed with 5 km raster. Bottom: RMSE for all subscenes inside the collocation radius from 1 km (subscene 2.4 × 2.4 km covers the buoy) to 100 km (blue) and for subscenes located directly on the collocation radius within a 10 km ring (red).

(subscenes approx. 2.4 × 2.4 km, buoy directly in the subscene) with approx. 5000 direct worldwide collocations up to 100 km with approx. 35 million collocations. The corresponding SWH RMSEs were analyzed.

In the first test, the uncertainties for all processed points inside the collocation radii were analyzed. The first row in Fig. 7 shows the number of subscenes collocated to the buoys as a function of the collocation radius. Note, for such an analysis, as all points inside the radius are evaluated, the RMSEs in distant areas were mostly compensated by the points near the buoys. For this case, the uncertainty starts with RMSE = 0.48 m directly on buoys and grows up to 0.66 m for collocations within 100 km (second row).

It can be concluded that each additional 1 km in the radius increases the integrated uncertainty by approx. 0.0018 m (1.8 cm for 10 km).

In the second test, the same radii were considered; however, only points inside a ring with a 10 km width were included. This approach excludes the influence of the points located near the buoys (third row). The uncertainties also start with RMSE = 0.48 m directly on buoys and grow up to 0.79 m for a 100 km collocation distance. This means that the extension of the collocation distance by 1 km produces an additional uncertainty of approx. 0.0032 m (3.2 mm, 3.2 cm for 10 km).

As a result, the following can be concluded regarding the SWH for S1 IW.

1) For a *point* with a certain distance to the buoy, the expected loss of accuracy is approx. 3.2 cm for each additional 10 km from the buoy (approx. 5%).
2) For a statistical analysis of the *database*, the expected loss of accuracy is approx. 1.8 cm for each additional 10 km extended collocation radius (approx. 2.5%).

C. *Processing and Improvement of S1 EW*

S1 EW are mostly acquired in polar regions; one product has swaths of approx. 450 km with approx. 400 km along-flight length (see Fig. 1). For the studies, EW data are processed with a raster of 17.5 km corresponding to approx. 400 datapoints per product (see Table VII). There are two types of ESA EW GRDs: GRDH (High resolution with 25 m pixel spacing) and GRDM (Medium resolution with 40 m pixel spacing), with GRDM amounting to around 80% of all products. During archive processing, it was found that the algorithm trained for GRDM data processes the EW GRDH products inaccurately. In the study, the model functions were retrained by including a product flag as an additional feature (0 = GRDH, 1 = GRDM). The new extended training datasets from 2014 to 2023 were created with approx. 70% GRDM and 30% GRDH data. Fig. 8 shows the validation of S1 EW with the whole archive 2024 by comparison with the MFWAM model and buoys. Compared to the model, the achieved RMSE = 0.45 m represents an improvement of approx. 15 cm compared to the previous study [2]. Table III shows the detailed analysis for SWH developed in the previous [2] (old) and in this study (new). For the buoy comparisons, the

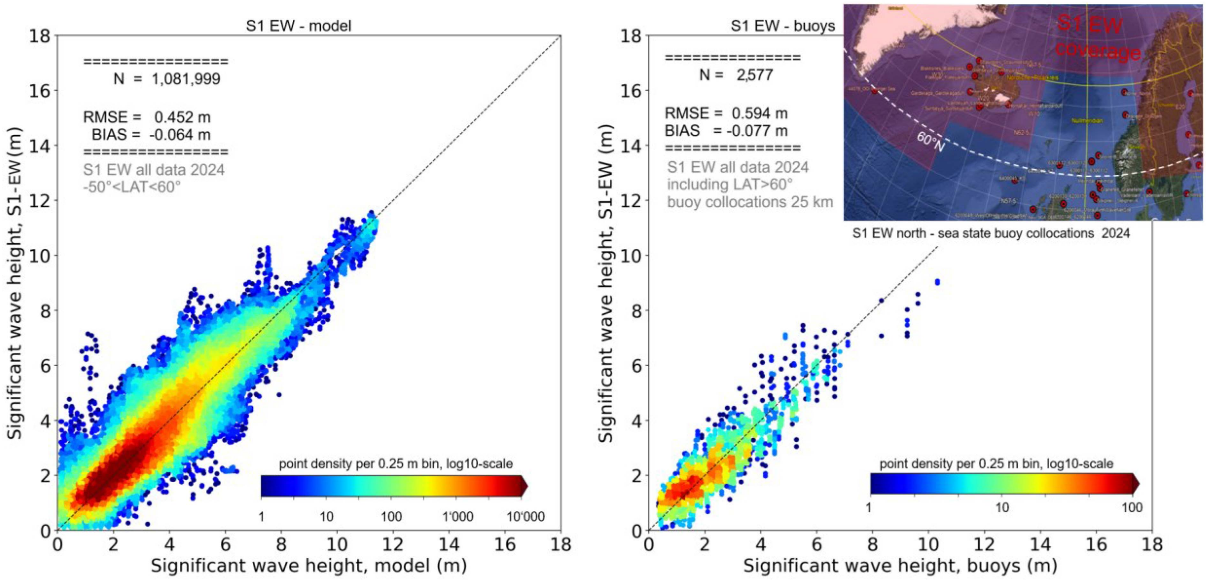

Fig. 8. S1 EW archive 2024 with approx. 26 000 scenes processed with a 17.5 km raster. Comparison with the MFWAM model (left) and buoys (right). The buoys collocated to EW acquisitions are located at LAT∼64°N around Iceland.

TABLE III
Analysis for SWH for S1 EW Archive 2024 Processed With 17.5 km Raster Using Model Functions Developed in Previous [2] (Old) and in This Study (New) Compared to MFWAM Model Results

Sea state domain (m)	RMSE (m)		BIAS (m)		N collocations (active points)	Data distribution %
	Old With [2]	**New This study**	Old With [2]	**New This study**		
0.0<SWH<1.5	0.60	**0.38**	–0.23	**–0.21**	232 444	21.47
1.5<SWH<3.0	0.42	**0.38**	–0.04	**–0.04**	610 995	56.44
3.0<SWH<6.0	0.82	**0.64**	0.08	**0.07**	220 696	20.39
6.0<SWH	1.48	**0.66**	0.11	**0.11**	18 341	1.69
TOTAL	0.61	**0.45**	–0.03	**–0.03**	1 082 476	100.00

area with LAT>60° should be considered as the only collocation opportunity. For buoys, RMSE = 0.59 m is reached. However, the small number of collocations for high sea states does not allow for a statistically justified analysis for individual domains, as shown in Table II for IW mode.

D. Processing of S1 WV

S1 WV are acquired in two parallel tracks (wv1, wv2) with imagettes approx. 20 × 20 km every 100 km along the satellite flight. The spatial extent of one product varies from around 1000 km (10 imagettes) to 16 000 km (160 imagettes) with a pixel resolution of approx. 3 m. Approx. 60 products per a day (both S1-A and S1–B) are acquired. From a technical perspective, the size of each S1 WV product, ranging from 2 to 10 GB (approximately 5 TB/month), each containing hundreds of compressed individual imagettes. The S1 WV data for 2014–2020 were already processed in the scope of ESA CCI-1 [2] and are publicly available [14]. In this work, the rest of the data 2021–2024 were processed and validated. The validation for SWH with the MFWAM model results in RMSE = 0.28 and 0.40 m for buoys. This is approx. 1.5 cm lower than the accuracy of the data 2014–2020 with respect to the model (BIAS of approx. 3 cm means lower S1 values in comparison to the model), but approx. 1.5 cm higher for buoys. However, it should be noted that the processing 2014–2020 included also approx. 10% of the data is used for training (especially storms).

Fig. 9 shows the validation of the processed S1 WV archive 2021–2024 with the MFWAM model and buoys (data 2014–2020 are available in [14] and published [10]). Table IV presents the detailed analysis of SWH for the four main sea state domains.

E. First Analysis of Sea State Estimated From Sentinel-1 Ten-Year Worldwide Archive

In the scope of the study, the first analysis of the SWHs distribution over a period of ten years was performed. This is an exemplary analysis showing the potential of the process data. Fig. 10 shows the monthly distribution of the sea state for each of four domains (0–1.5, 1.5–3, 3–6, >6 m) with each S1 mode representing different acquisition areas: open oceans (S1 WV), shelf and seas (S1 IW), and polar regions (S1 EW). The seasonal change is well visible, where the number of storms and, accordingly, the high waves decrease, and the percentage of low waves increases in the northern summer periods. The ten-year

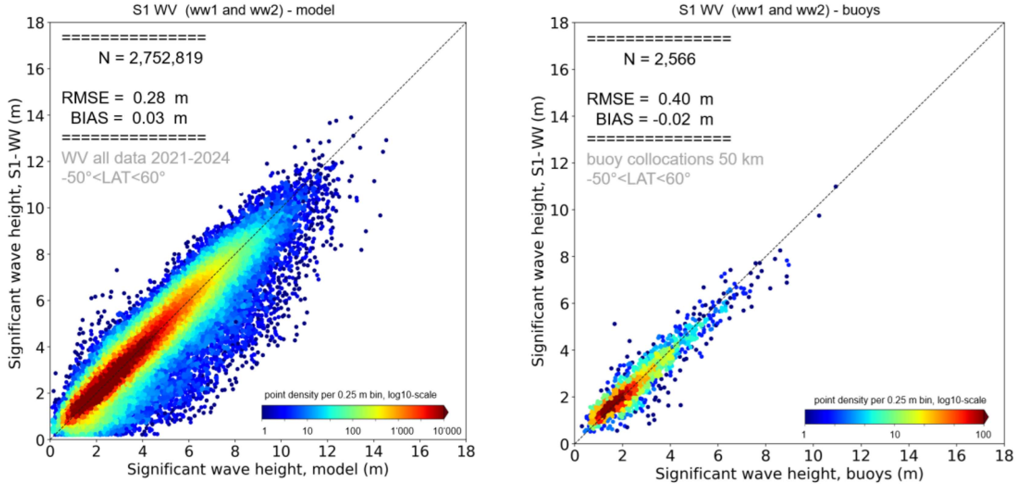

Fig. 9. S1 WV archive 2021–2024 (2014–2020 published in [12] and available in [13]). Comparison with the MFWAM model (left) and buoys (right).

TABLE IV
ANALYSIS OF THE SWH FOR THE PROCESSED S1 WV ARCHIVE 2021–2024

Sea state domain (m)	RMSE (m)		BIAS (m)		model		buoys	
	Model	Buoys	Model	Buoys	N collocations	Data distribution %	N collocations	Data distribution %
0.0<SWH<1.5	0.24	0.29	–0.13	–0.19	330 244	11.97		
1.5<SWH<3.0	0.23	0.36	–0.03	–0.02	1 749 144	63.39	1377	53.68
3.0<SWH<6.0	0.36	0.55	0.01	0.14	637 088	23.09	450	17.54
6.0<SWH	0.84	0.73	0.17	0.41	43 068	1.56	55	2.14
TOTAL	**0.28**	**0.40**	**–0.03**	**–0.03**	**2 759 544**	**100.00**	**2565**	**100.00**

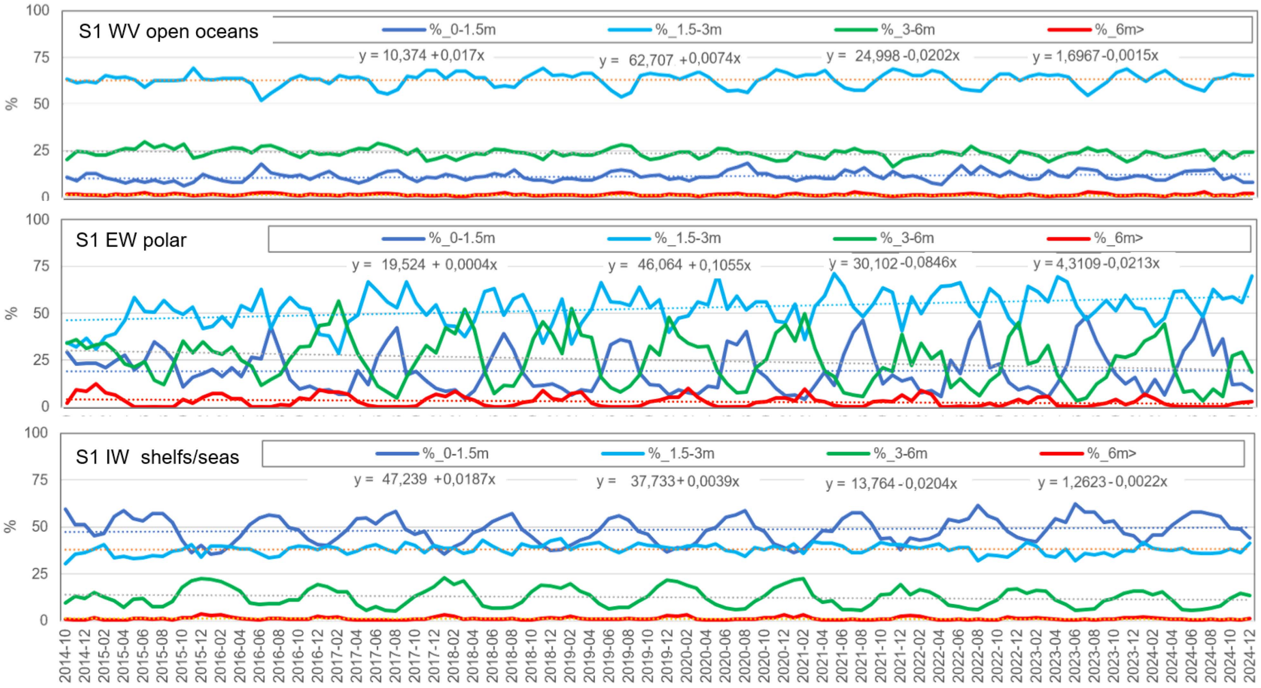

Fig. 10. Monthly distribution of all S1 data 2014–2024 for four sea state domains: SWH 0–1.5 m (slight), 1.5–3 m (moderate), 3–6 m (rough), SWH>6 m (high). Trendlines present the percentage of SWH in a domain, where *x* means the *n*-month period since October 2014.

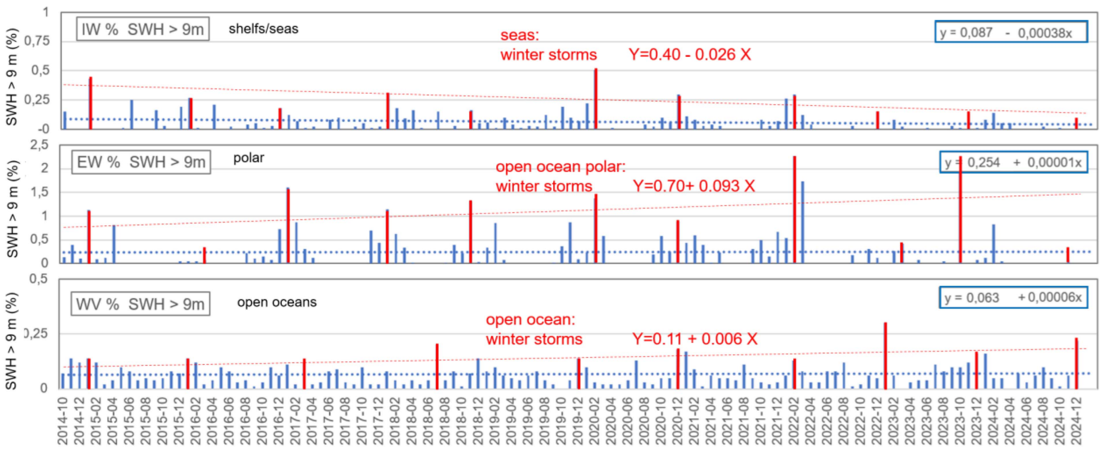

Fig. 11. Monthly distribution of extreme storms with SWH>9 m in all S1 data 2014–2024. The blue trendlines present the percentage of SWH (*x* means the month since October 2014). For ten years, the WV acquisitions in the open ocean depict an average increase approx. 0.01% of the total percentage (approx. 20% of its relative value in 2014), EW acquisitions in polar regions depict a weak increase of approx. 0.001% of the total sea state and the shelf regions and seas acquired by IW depict a decrease of approx. 0.05%. Additionally, the intensity of winter storms increases in WV and EW acquisitions for open oceans (red trend lines for max, *X* means year since 2014).

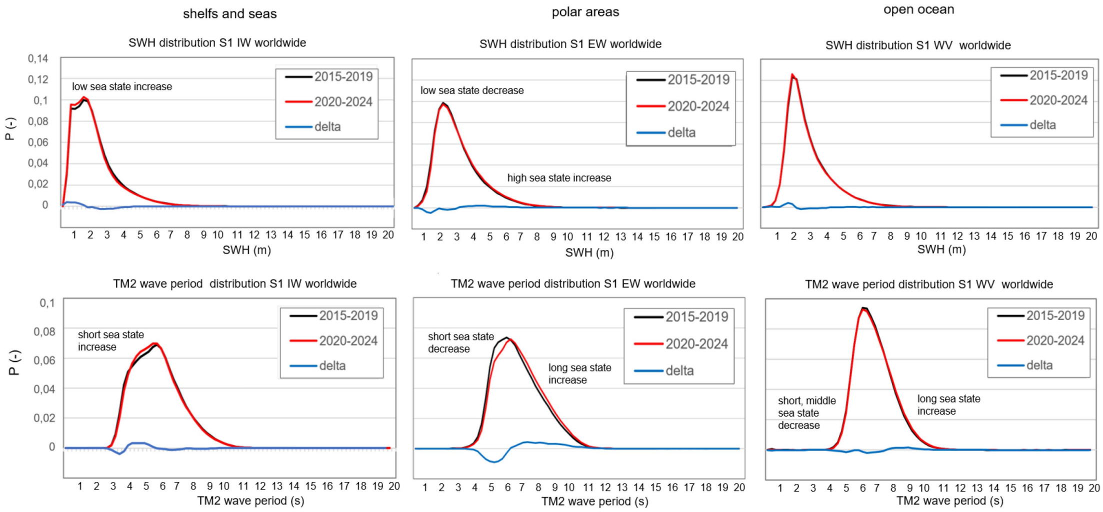

Fig. 12. Total distribution of SWH and TM2 period in ten years of S1 data divided into two five-year subsets: 2015–2019 and 2020–2024. For shelf and seas (IW): the increase of the low sea state SWH<2.5 m with decreasing of very-short waves with TM2<4 s, but increasing for middle-short waves within the range 4<TM2<6 s. For open-ocean (WV): no significant change of SWH, light decrease of the short waves with TM2<6 s and light increase for longer waves with TM2>6 s. For polar regions (EW): decrease of the low sea state SWH<2.5 m with a light increase for SWH>2.5 m and a strong decrease of the short waves TM2<6 s with an increase for TM2>6 s.

trends are positive for low sea state with an increase of approx. 2% of the total value and negative for high sea state, with a decrease of approx. 2% for all three S1 modes.

However, these distributions give only a total overview and do not depict the intensity of the storms and the local redistribution of the sea state conditions in different regions by storms. To do this, more precise analyses can be carried out using archive data. Fig. 11 demonstrates the monthly distribution of extreme storms with SWH>9 m ["very high" according to the World Meteorological Organization (WMO) sea state scale] in all S1 data. For ten years, the WV acquisitions in the open ocean depict an average relative increase of approx. 0.3% of the total percentage of SWH>9 m. EW acquisitions in polar regions also depict an increase of approx. 0.001% of sea state. IW acquisitions in shelf regions and seas depict a decrease of approx. 0.05%. Additionally, the intensity of winter storms increases in WV and EW acquisitions in open oceans.

To analyze the temporal variations, the 10-year data were divided into two five-year subsets: 2015–2019 and 2020–2024. Fig. 12 presents the total distribution PDF (probability distribution function built with 0.25 m bins) of SWH and TM2 for these two five-year subsets. For shelf and seas (S1 IW), an increase of the low sea state SWH<2.5 m with a decrease of very short waves with TM2<4 s, but an increase for intermediate-short waves with TM2 between 4 and 6 s can be observed.

For open-ocean (WV), no significant change of SWH, but a slight decrease of the short waves with TM2<6 s and a slight increase for longer waves with TM2>6 s has been found. For polar regions (EW), a decrease of the low sea state SWH<2.5 m with a slight increase for SWH>2.5 m and a strong decrease of

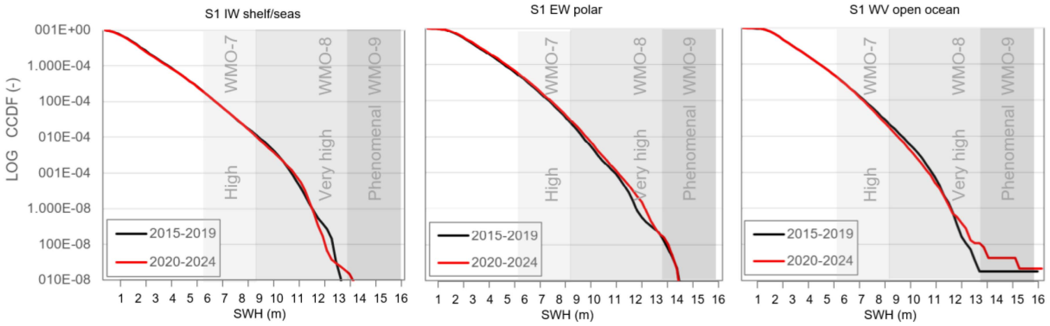

Fig. 13. CCDF displays statistics for sea state over a certain SWH value for S1 IW (shelf/seas), S1 EW (polar), and WV (open-ocean) acquisitions in ten years of S1 data divided into two five-year subsets: 2015−2019 and 2020−2024. Log-scale shows the differences in the high sea state domain with SWH>9 m. In shelf and seas, the number of high SWHs decreases; in open ocean and polar regions, it increases.

the short waves TM2<6 s with an increase for TM2>6 s can be noticed.

The Complementary Cumulative Distribution Function (CCDF, equal to “1-CDF” Cumulative Distribution Function) accumulates cases with SWH above a certain threshold value. The CCDF sensitively reflects changes in all regimes, especially in very rough sea conditions. Fig. 13 shows the log-scaled CCDFs for all three modes and two data subsets: 2015−2019 and 2020−2024. The number of high SWHs decreases in the shelf and seas (IW), whereas it increases in the open ocean and polar regions.

In general, based on the S1 data it can be concluded that in the last ten years the total worldwide sea state including seas (Mediterranean, Baltics, Black Sea, Caspian Sea, etc.) has a slight increase in the percentage of low sea state with a corresponding decrease in high sea by about 2% of the total in shelf areas and seas (Mediterranean, North, Baltic, Black Seas, etc.), but an increase in very high storms on the open ocean by about 0.3% in the last ten years. However, a dominant amount of S1 IW and EW scenes are acquired in the North Atlantic: to one 0.2° raster point on the globe approx. 300−500 processed SWH values are assigned per year (in other regions, e.g., Africa and south America only up 100 times per a year, see Fig. 2).

The results of a decrease in the SWH in the North Atlantic region agree with other scientific studies on climate research. For example, numerical studies simulating the future sea state distribution based on different scenarios report: “of the end of 2060 …ongoing climate change acts not only to increase SWH and wind speed, but also to significantly decrease them regionally. For example, in the North Atlantic and South Pacific (between 140°E and 130°W), continuously decreasing linear trends (negative detection) in the SWH are projected in the future …” [30].

F. *First Spatial Analysis From Sentinel-1 Ten-Year Worldwide Archive*

The S1 data can also be applied for a spatial analysis of geophysical changes in sea state and energy redistribution. In addition to the models, this enables, for the first time, to evaluate the worldwide changing of the sea state conditions and wave energy fluxes (power transported by waves), including not only open oceans (already possible using, e.g., altimeters and earlier SAR missions) but also including shelf areas and closed seas like the Mediterranean Sea. Fig. 14 presents the changes in the worldwide mean SWH and wave energy fluxes projected on a 5° mesh based on five-year averaged values from 2015 to 2019 and 2020−2024. For this, the wave energy flux F was assessed in simplified form as the product of total integrated wave energy density per unit area E_w and wave group velocity C_g as $F = E_w{\cdot}C_g$ [W/m], where the energy density E_w (sum of kinetic and potential) can be estimated from the wave height with $E_w = (1/8)\rho{\cdot}g{\cdot}\mathrm{SWH}^2$ (ρ means water density and g the Earth’s acceleration). The group velocity can be approximated using the mean wave period $C_g = (g/4\pi)T_{mean}$ estimated also from SAR.

S1-based data show a slight increase in the north of the North Atlantic by approx. 10 kW/m, a decrease in its central part by approx. 20 kW/m, and a strong increase in its western part by about 40 kW/m. Also, it can be clearly seen that the storms near Cape of Good Hope in South Africa became lower and contained less energy, while storms off Cape Horn in South America intensified.

However, ten years is a very short period for a single data source for fully reasoned geophysical statements. When the data are combined with data from other SAR satellites such as ENVISAT-ASAR (2002−2012) and ERS (1989−2000) and other instruments such as altimeters, in-situ measurements (buoys), and also hindcast data (an example difference between two models was shown in Section II), a much more realistic view of the circumstances will be possible. Enabling this is the goal of the ESA CCI initiative.

G. *Example Analysis of Individual Storms Analysis*

The processed archive can be applied to studies of the long-term worldwide statistics, but it can also be employed for analysis of the individual local storm developments. Fig. 15 presents an example of the S1-A estimated sea state for a huge storm in the North and Baltic Seas in October 2023, which caused a series of damage and destruction in the coastal areas.

The registered SWH reached approx. 9.5 m (“Very high” 8 according to WMO sea state scale). Over the four days of the storm peak from 2023-10-19 to 2023-10-22, 14 scenes with 74 individual S1 IW product IDs were acquired in the area. For three days (19th, 20th, 22nd), both morning descending

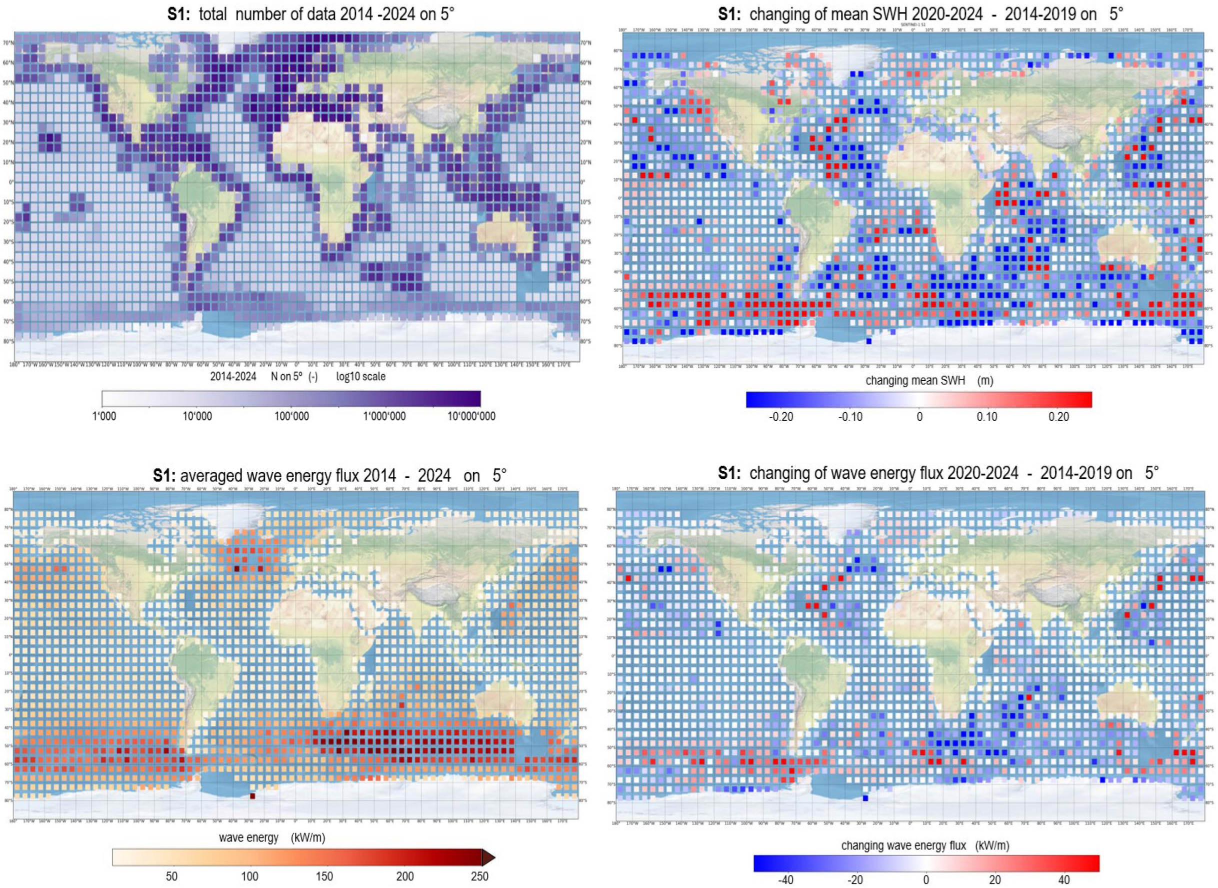

Fig. 14. Number of all processed data 2014–2024 (top left) and averaged wave power estimated from S1 (bottom left) projected on a mesh of 5°. Changing of mean SWH (top right) and wave power (bottom right) based on data averaged for two five-year data 2020–2024 and 2014–2019.

(04:00 – 07:00 UTC) and evening ascending (between 15:00 and 18:00 UTC) passes are acquired. Due to the offset of the satellite track (repeating cycle 12 days), only two scenes in the area were recorded on 2023-10-21. Fig. 16 shows an example one-month timeseries (S1 IW, model, buoys) for two locations (shown as red dots in Fig. 15 in the upper left image): in the middle of the North Sea and in the German Bight near the coast. The storm peak is marked with magenta color. In both, Figs. 15 and 16, it can be seen that the storm peak with SWH>6 m in the North Sea on 2023-10-19 has a time delay in the model (06:04 and 15:40 UTC acquisitions) and is covered by S1 IW only two days later on 2023-10-21 in S1 IW acquired at 05:48 UTC. In the southern Baltic Sea, the peak with SWH>3 m matches in the model and S1 IW spatially and temporally.

This example shows that, although the model prediction is correct, in this case, it is late by several hours in the North Sea. In areas without buoys, where it is only possible to work with model predictions, information from satellites can provide an additional verification of the forecast data. Depending on the class of the ship, certain sea conditions can be dangerous and lead to the loss of cargo. Furthermore, driving ships against currents and waves significantly increases resistance and thus fuel consumption [30]. In this way, processing and delivering the SAR data in NRT can help the ship's crew in safe and economic navigation.

IV. SUMMARY AND OUTLOOK

The study presented in this article constitutes the first complete sea state dataset and analysis of 10 years of S1 data, comprised of all available significant acquisition modes (see Fig. 1). The data volume of approx. 4.2 million scenes and approx. 3.3 billion data points are unprecedented and provide a solid statistical basis for studies on, e.g., possible climate change impacts on sea state. In comparison to all previous studies, the processed data cover not only the open ocean, but also shelves and all internal seas.

The results will be incorporated into the climate studies planned at ESA CCI. These will be combined with other data sources processed from the same archive using alternative methods developed by other institutions, as well as data from other instruments, e.g., altimeters. In this way, the statistical distribution of the sea state and the change in the global circumstances can be better quantified.

As the time coverage of the S1 mission is limited to only 10 years, a special topic of CCI is the combination of S1 data with data from preceding global SAR missions, first of all with ENISAT-ASAR 2002–2012 [32]. A joint product of both missions can already cover a quarter of a century and will show more accurate and better statistically justified trends of climate change impacts on sea state redistribution.

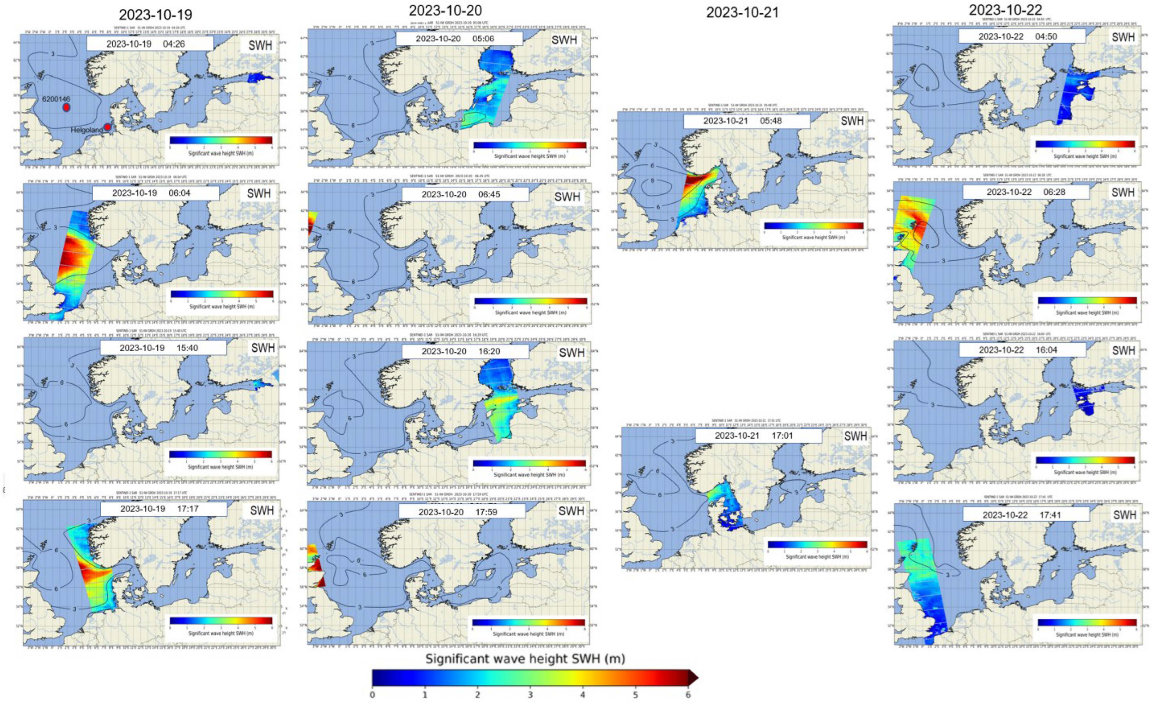

Fig. 15. Example of sea state from S1 IW acquisitions during a heavy storm in the North and Baltic Seas in October 2023: 14 S1 IW scenes with 74 individual S1 IW products. The isolines represent the model (output every 3 h, model time closest to the acquisition is shown). The storm peak with SWH>6 m in the North Sea on 2023-10-19 has a time delay in the model (06:04 and 15:40 UTC acquisitions) and is covered by S1 IW only two days later on 2023-10-21 in S1 IW acquired at 05:48 UTC. In the southern Baltic Sea, the peak with SWH>3 m matches in the model and S1 IW spatially and temporally.

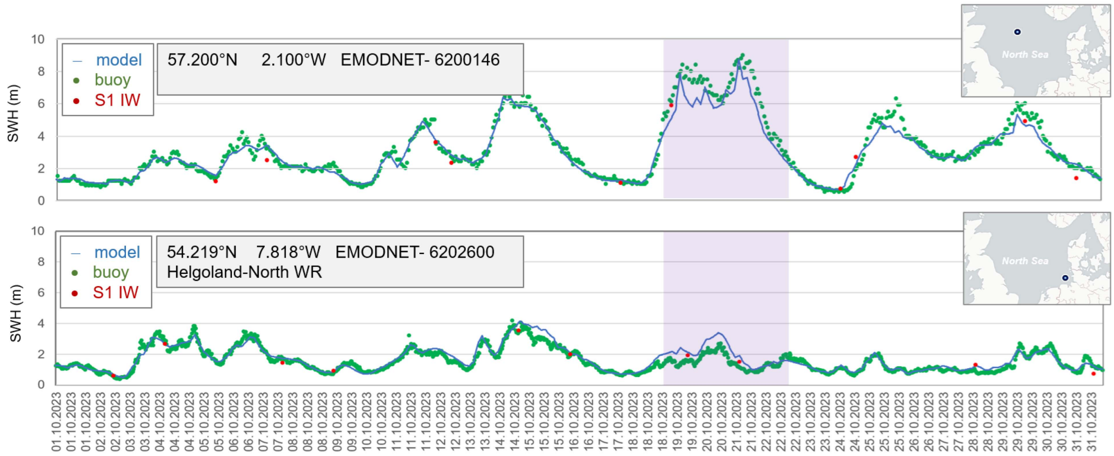

Fig. 16. Example of a one-month timeseries for October 2023: S1 IW, model, and buoys for two locations (shown as red dots in Fig. 15 in the upper left image) representing the center of the North Sea and German Bight near the coast. The storm peak 2023-10-19–2023-10-22 is marked with magenta color.

The ten-year SWH analysis based on the processed S1 archive shows that the total sea state in the acquisition areas has an increase in low sea state, a slight decrease in high sea state percentage, with approx. 2%, but an increase in storm intensities. These results are covered by other scientific studies on climate research predicting also a redistribution of the global sea state with a slight decrease of SWH in the North Atlantic until 2060 [31]. Spatially, S1-based data show an increase of storm intensity in the north of the North Atlantic and a decrease in its central part: The storms by Cape of Good Hope in South Africa became lower and contained less energy, while storms off Cape Horn in South America intensified.

In terms of the algorithm, this is the first time that a large amount of processed data has been allowed to be used for buoy collocations for training purposes in a large volume, with a total amount of 0.5 million data points. It was also shown that the ground truth model data have different worldwide uncertainties and should be selected in the areas with lower uncertainty. It was

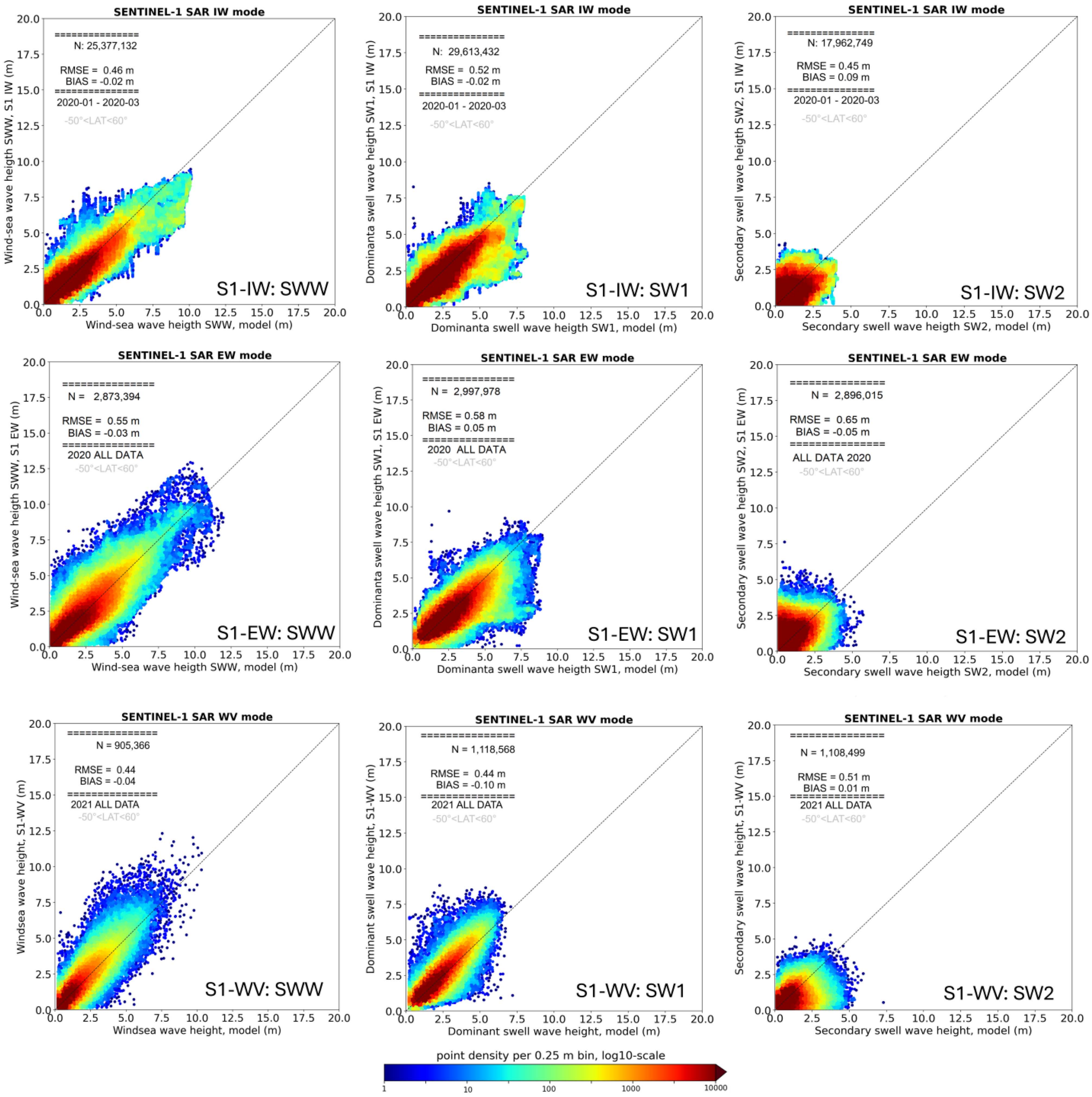

Fig. 17. Comparison of partially integrated wave height with MFWAM model results for S1 IW (first line), EW (second line), and WV (last line): windsea SWW (first column), dominant swell SW1 (middle column), and secondary swell SW2 (right column). Only nonzero values are considered.

TABLE V
Total RMSEs for Integrated Sea State Parameters for SAR-SeaStaR Algorithm

Parameter	Abb.	Unit	Satellite mode		
			S1 IW	S1 EW	S1 WV
Total significant wave height	SWH	m	**0.38**	**0.45**	0.28
Mean wave period	TM0	s	0.88	0.92	0.50
First moment wave period	TM1	s	0.97	0.85	0.55
Second moment wave period	TM2	s	0.96	0.86	0.49
Wave height swell dominant system	SW1	m	**0.52**	**0.58**	0.44
Wave height swell secondary system	SW2	m	0.45	0.65	0.51
Significant wave height windsea	SWW	m	**0.46**	**0.55**	0.44
Mean period windsea	TMW	s	0.97	0.95	0.65

TABLE VI
UNCERTAINTIES FOR TOTAL SWH AND PERCENTAGE OF NONVALID DATA

	Number of processed S1 products in DLR_OCN		
	S1 WV	S1 IW	S1 EW
SAR product	SLC	GRDH	GRDH/GRDM
Pixel spacing, m	3.5	10	25 / 40
RMSE model, m	0.28	0.38	0.45
RMSE buoys, m	0.40	0.40	0.59
Nonvalid, %	1.5	6.3	5.1

determined that the areas of the west coast of Africa, the Middle America, as well as around India, the Philippines, and eastern Australia should be avoided by the creation of the training data sets, as these are areas with increased uncertainties. Both factors allowed for improvement in the accuracy to an RMSE of 0.38 m with respect to 0.42 m in the previous study using the same model approaches and SAR features [2]. Table V summarizes the state-of-the-art averaged values for the uncertainties based on [2] with updates from this study (in bold). Additionally, Fig. 17 demonstrates a comparison of the swell and windsea components with the MFWAM model. For S1 IW and EW, the dominant swell SW1 and windsea SWW are also improved with ML SVM models.

In terms of accuracy and nonprocessed data, by processing all available worldwide scenes, the RMSEs reached a relatively low percentage of invalid values (only water points). For example, to reach the same accuracy for WV, comparable algorithms [13], [15] reject 10.8% of the data as nonvalid against 1.5% in this study. Table VI presents the uncertainties and percentage of invalid data for all three modes for the ice-free validation area $-50^\circ < \mathrm{LAT} < 60^\circ$. The model comparisons are conducted worldwide, and the buoys are located dominantly in shelves (S1 EW all buoys $\mathrm{LAT} > 60^\circ$ as only one possibility). The uncertainties are dependent on the area of acquisition (open ocean with swell and high sea state, coastal zones with short sea state, and artifacts like ships and offshore constructions), but more directly on the SAR-mode with different pixel spacing.

In terms of future techniques, the onboard processing has already been developed for direct installation on a satellite [33]. In this case, processed sea state parameters can be directly transferred from satellite to Earth for NRT services. This technology will also significantly reduce the delay of sea state products delivery in NRT. As an application, using SAR data in NRT can help the ship's crew with safe and economic navigation [31].

APPENDIX

See Table VII and VIII.

TABLE VII
SENTINEL-1 IW, EW, AND WV PRODUCTS MAIN CHARACTERISTICS AND PROCESSING PERFORMANCE (2020, BOTH S1A AND S1B IN SERVICE)

Satellite Mode	IW	EW	WV
Main area of acquisition	Shelf, seas, coastal	Polar, Madagascar, Atlantic	Open ocean
Product type	GRD (GRDH)	GRD (GRDH, GRDM)	SLC
ID product coverage	Approx. 250×200 km	Approx. 450×400 km	Along-orbit imagettes approx. 20×20 km each 100 km
Product pixel spacing	10 m	40 m (GRDM), 25 m (GRDH)	Approx.3.5 m
Averaged ID product memory size	Approx. 2 GB (0.5 GB – 4 GB)	Approx. 0.7 GB (0.2 GB – 2 GB)	Approx. 7 GB (2 GB – 16 GB)
Total worldwide ID products/day (S1A and S1B 2020)	Approx. 900	Approx. 260	Approx.60 products with approx. 5400 imagettes
Ocean scenes products/day (S1A and S1B in 2020)	Approx. 400	Approx. 200	Approx.60 products with Approx. 5400 imagettes
Products/year ocean scenes (S1A and S1B in 2020)	Approx. 150 000	Approx. 72 000	Approx.21 000 products with approx. 16 Mio imagettes
Processing raster	5 km	17.5 km	Each 100 km along flight
Number of processed subscenes/product	Approx. 1500 (100% water)	Approx. 450 (100% water)	Approx. 100 (20 – 180)
Processed ocean products/ subscenes per year (2020)	Approx. 310 000/ approx. 140 million	Approx. 95 000/ approx. 40 million	Approx. 35 000 approx. 1 million

TABLE VIII
PROCESSED OCEAN PRODUCT ID EXCLUDING LAND SCENES (2014 ONLY OCTOBER–DECEMBER S1-A, 2017–2022 S1-A AND S1-B, 2022–2024 ONLY S1-A)

Year	Number of processed S1 products in DLR_OCN		
	S1 IW	S1 EW	S1 WV
2014	7453	6954	85
2015	46 476	36 977	4257
2016	71 033	54 468	16 780
2017	154 712	70 352	24 425
2018	170 763	72 255	24 955
2019	176 788	78 894	23 501
2020	183 223	75 724	22 415
2021	183 413	67 034	21 513
2022	110 998	25 684	9911
2023	111 267	25 212	10 574
2024	113 031	25 674	14 512
Total	**1 329 157**	**539 228**	**172 928**

REFERENCES

[1] European Space Agency (ESA), "Overview of Sentinel-1 mission," Accessed: Mar. 2026. [Online]. Available: https://sentiwiki.copernicus.eu/web/s1-mission

[2] A. Pleskachevsky, B. Tings, S. Jacobsen, S. Wiehle, E. Schwarz, and D. Krause, "A system for near-real-time monitoring of the sea state using SAR satellites," *IEEE Trans. Geosci. Remote Sens.*, vol. 62, 2024, Art. no. 5219018, doi: 10.1109/TGRS.2024.3419582

[3] IFREMER, "Algorithm level-1 SLC to level-1B XSP cross spectrum Sentinel-1," 2024. [Online]. Available: https://cerweb.ifremer.fr/datarmor/sarwave/documentation/processor/sar/xsarslc/html/ATBD.html

[4] J. Schulz-Stellenfleth, T. König, and S. Lehner, "An empirical approach for the retrieval of integral ocean wave parameters from synthetic aperture radar data," *J. Geophys. Res., Oceans*, vol. 112, no. C3, p. 14, 2007.

[5] A. Pleskachevsky, S. Jacobsen, B. Tings, and E. Schwarz, "Estimation of sea state from Sentinel-1 synthetic aperture radar imagery for maritime situation awareness," *Int. J. Remote Sens.*, vol. 40, no. 11, pp. 4104–4142, Jun. 2019.

[6] S. Abdalla, J. R. Bidlot, and P. Janssen, "Global validation and assimilation of ENVISAT ASAR wave mode spectra," in *Proc. SeaSAR*, 2006, vol. 613, p. 6.

[7] S. Abdalla, J. Bidlot, and P. Janssen, "Envisat ASAR wave mode spectra global validation and assimilation," in *Proc. SeaSAR*, 2010, vol. 679, pp. 25–29.

[8] W. Alpers and C. Rufenach, "The effect of orbital motions on synthetic aperture radar imagery of ocean waves," *IEEE Trans. Antennas Propag.*, vol. AP-27, no. 5, pp. 685–690, Sep. 1979, doi: 10.1109/TAP.1979.1142163.

[9] B. Holt, "SAR imaging of the ocean surface. In: Jackson, C.R., Apel, J.R. (Eds.), synthetic aperture radar (SAR)," in *Marine User's Manual*, Washington, DC, USA: NOAA NESDIS Office of Res. and Appl., 2004, pp. 25–79.

[10] A. Pleskachevsky, B. Tings, S. Wiehle, J. Imber, and S. Jacobsen, "Multiparametric sea state fields from synthetic aperture radar for maritime situational awareness," *Remote Sens. Environ.*, vol. 280, Oct. 2022, Art. no. 113200.

[11] S. Voinov, E. Schwarz, D. Krause, and B. Tings, "Earth observation maritime surveillance system," in *Proc. GeoForum MV*, 2020, pp. 73–77.

[12] J. E. Stopa and A. Mouche, "Significant wave heights from Sentinel-1 SAR: Validation and applications," *J. Geophys. Res., Oceans*, vol. 122, no. 3, pp. 1827–1848, Mar. 2017.

[13] B. Quach, Y. Glaser, J. E. Stopa, A. A. Mouche, and P. Sadowski, "Deep learning for predicting significant wave height from synthetic aperture radar," *IEEE Trans. Geosci. Remote Sens.*, vol. 59, no. 3, pp. 1859–1867, Mar. 2021, doi: 10.1109/TGRS.2020.3003839.

[14] A. Pleskachevsky and B. Tings, "ESA sea state climate change initiative (Sea_State_CCI): Global remote sensing multi-mission along-track integrated sea state parameters (ISSP) from SAR WV onboard Sentinel-1A & 1B, L2P product, release version 3," NERC EDS Centre for Environmental Data Analysis, 2022, doi: 10.5285/fe02d5eef9ef4ad889d1917ccad3b35f.

[15] A. Grouazel, J. Stopa, J.-F. Piollé, A. Mouche, and P. Sadowski, "ESA sea state climate change initiative (Sea_State_cci): Global remote sensing multi-mission along-track significant wave height (SWH) from SAR WV onboard Sentinel-1A & 1B, L2P product, release version 3," NERC EDS Centre for Environmental Data Analysis, 2022, doi: 10.5285/81bab8b378db443db4482a5961a58ec1.

[16] H. Wang et al., "Quad-polarimetric SAR sea state retrieval algorithm from Chinese Gaofen-3 wave mode imagettes via deep learning," *Remote Sens. Environ.*, vol. 273, 2022, Art. no. 112969.

[17] J. Morim et al., "A global ensemble of ocean wave climate projections from CMIP5-driven models," *Nature Sci. Data*, vol. 7, pp. 711–721, 2020, doi: 10.1038/s41597-020-0446-2.

[18] J. Morim et al., "Robustness and uncertainties in global multivariate wind-wave climate projections," *Nature Climate Change*, vol. 9, pp. 711–718, 2019, doi: 10.1038/s41558-019-0542-5.

[19] F. Ardhuin et al., "Semi-empirical dissipation source functions for wind-wave models: Part I, definition, calibration and validation at global scales," *J. Phys. Oceanogr.*, vol. 40, pp. 1917–1941, Jan. 2010.

[20] NOAA. Accessed: Mar. 2026. [Online]. Available: https://polar.ncep.noaa.gov/waves/

[21] NDBC. Accessed: Mar. 2026. [Online]. Available: https://www.ndbc.noaa.gov/

[22] LRZ, Leibniz supercomputing centre. Accessed: Mar. 2026. [Online]. Available: www.lrz.de

[23] European Space Agency (ESA), "Climate change initiative CCI," Accessed: Mar. 2026. [Online]. Available: https://climate.esa.int/en/#/

[24] CMEMS, "Copernicus marine environment monitoring service," Accessed: Mar. 2026. [Online]. Available: https://marine.copernicus.eu/

[25] ECCC. Accessed: Mar. 2026. [Online]. Available: http://www.medssdmm.dfo-mpo.gc.ca/isdm-gdsi/waves-vagues/index-eng.htm

[26] EMODnet. Accessed: Mar. 2026. [Online]. Available: http://www.emodnet-physics.eu/Map/#

[27] C.-C. Chang and C.-J. Lin, "Training v-support vector regression: Theory and algorithms," *Neural Comput.*, vol. 14, no. 8, pp. 1959–1977, Aug. 2002.

[28] Z. Wen, J. Shi, Q. Li, B. He, and J. Chen, "ThunderSVM: A fast SVM library on GPUs and CPUs," *J. Mach. Learn. Res.*, vol. 19, no. 21, p. 5, 2018.

[29] H. Hersbach, "CMOD5.N: A C-band geophysical model function for equivalent neutral wind," ECMWF, Tech. Rep., 2008.

[30] M. Dobrynin, J. Murawski, J. Baehr, and T. Ilyina, "Detection and attribution of climate change signal in ocean wind waves," *J. Climate*, vol. 28, pp. 1578–1586, 2015.

[31] A. Ioannou, E. Moschos, B. L. Vu, and A. Stegner, "Short-term optimal ship routing via reliable satellite current data," in *Proc. SNAME 8th Int. Symp. Ship Operations, Manage. Econ.*, 2023, p. 6, doi: 10.5957/SOME-2023-044.

[32] X. M. Li and B. Huang, "A global sea state dataset from spaceborne synthetic aperture radar wave mode data," *Sci. Data*, vol. 7, p. 12, 2020, doi: 10.1038/s41597-020-00601-3.

[33] S. Wiehle, S. Mandapati, D. Günzel, H. Breit, and U. Balss, "Synthetic aperture radar image formation and processing on an MPSoC," *IEEE Trans. Geosci. Remote Sens.*, vol. 60, 2022, Art. no. 5226814.

Andrey Pleskachevsky received his Diploma in hydropower engineering from Technical University St. Petersburg in 1994 with focus on hydrodynamic numerical modelling and data analyses. His PhD in 1999 was performed at GKSS-Research Center (today Helmholtz Center HERION) where he was working on spectral wave modeling and coupling of waves, circulation and suspended matter transport models as well as implementation of satellite data into modelling until 2009. In 2009 he joined the Remote Sensing Technology Institute at the German Aerospace Center (DLR) where he develops algorithms for retrieval the meteo-marine parameters from synthetic aperture radar for near-real-time services.

Björn Tings received the bachelor's degree in scientific programming from FH Aachen and his simultaneous qualification in mathematical-technical software development from RWTH Aachen University, Aachen, Germany, in 2010, the master's degree in artificial intelligence from Maastricht University, Maastricht, Netherlands, in 2013, and the Ph.D. degree from Helmut Schmidt University, Hamburg, Germany, in 2025 in Remote Sensing and SAR-oceanography.

Christoph Schnupfhagn received the Ph.D. degree in physics from the University of Bayreuth, Bayreuth, Germany, in 2023, in the field of optical spectroscopy.

He joined the Maritime Safety and Security Lab in Bremen, which is part of the Remote Sensing Technology Institute (IMF) at the German Aerospace Center (DLR). He focuses on the development of algorithms that can automatically extract parameters about the ocean surface from SAR satellite data. These include the detection and drift modeling of oil pollution and the interferometric detection and analysis of landfast ice.

Stefan Wiehle received the diploma in physics and the Dr. rer. nat. degree from the Technical University of Braunschweig, Braunschweig, Germany in theoretical physics, in 2010 and 2014, respectively.

He works with the DLR Maritime Safety and Security Lab in Bremen, a group at DLR's Remote Sensing Technology Institute (IMF). His focus is on the implementation and automation of SAR maritime value-added algorithms such as land-water-line detection, bathymetry derivation, or sea ice classification. He also led DLR's activities in several research projects.

Sven Jacobsen received the Ph.D. degree in geophysics at University of Cologne in the field of space plasma physics and fluid dynamics in 2011. Since then, he has been working in the area of oceanography and remote sensing

Since then, he has been working in the area of oceanography and remote sensing. In 2013, he joined DLR and became head of the Maritime Safety and Security Center Bremen in 2016. He and his team work on the development of software algorithms to derive maritime information (wind fields, sea state, oil-, ship-, and iceberg detection, etc.) from satellite data.